Carbohydrate Research 492 (2020) 107990

Contents lists available at ScienceDirect

Carbohydrate Research

journal homepage: www.elsevier.com/locate/carres

Design, synthesis, characterization and biological evaluation of Thieno[2,3−*b*]pyridines−chitosan nanocomposites as drug delivery systems for colon targeting

Hanaa Mansour*, Ahmed I. Khodair, Samia M. Elsiginy, Amal E. Elghanam

Department of Chemistry, Faculty of Science, Kafrelsheikh University, Kafrelsheikh, 33516, Egypt

ARTICLE INFO

Keywords:
Thienopyridines
Chitosan
Nanocomposites
Drug release
Antibacterial
Colon targeting

ABSTRACT

Thieno[2,3−*b*]pyridine derivatives **DATP$_{a-c}$** have been synthesized based on Thorpe−Ziegler Cyclization. The reaction of arylidene malononitrile derivatives (**I$_{a-c}$**) with thiocyanoacetamide (**II**) in basic medium (piperidine) followed by alkylation using ethyl chloroacetate and finally, cyclization in sodium ethoxide yielded **DATP$_{a-c}$**. Thieno[2,3−*b*]pyridine−chitosan nanocomposites **CS−DATP$_{a-c}$** were prepared from the **DATP$_{a-c}$** and **CS** nanoparticles using sodium tripolyphosphate (TPP). **CS−DATP$_{a-c}$** nanocomposites were characterized using FTIR, TEM and XRD techniques and showed a relatively narrow size distribution of monodispersed nanoparticles with the average size of 14–78 nm. The *in vitro* release studies of **CS−DATP$_{a-c}$** nanocomposites were investigated and showed that the drug release rate is pH-dependent and the trend is as follows: basic > neutral > acidic. The faster release rate in basic medium effectively prolongs drug delivery in gastric pH. Additionally, the antibacterial investigation showed that **DATP$_{a-c}$** and **CS−DATP$_{a-c}$** nanocomposites exhibited antibacterial activity against both Gram-positive and Gram-negative bacteria but **CS−DATP$_{a-c}$** nanocomposites showed much higher antibacterial activity compared to the **DATP$_{a-c}$**, which in agreement with the particle size measurements as **DATP$_{a-c}$** are in the bulky structure whereas, **CS−DATP$_{a-c}$** are in the nanostructure. The results may have applications of drug design for colon targeting.

1. Introduction

Chitosan (CS), a biopolymer, has been largely studied as a pharmaceutical excipient for colon-specific delivery [1,2]. The advantages of CS are biocompatibility, nontoxicity, biodegradability, antibacterial activity, low cost and ease of chemical modifications. It has been examined extensively in the pharmaceutical industry for the development of a drug delivery system [3]. CS nanoparticles are used as drug carriers and showed controlled drug release, however, the low water-solubility under physiological pH was the main disadvantage [4]. To overcome this limitation, many composite/nanocomposite of chitosan with other compounds have been designed and investigated and showed new properties via the interaction of the constituents [5,6].

Thieno[2,3−*b*]pyridines, reported for the first time in 1913 [7], are important fused heterocyclic compounds [8] and have a broad spectrum of biological activities [9]. Some of them possess cytotoxic activity [10–14] anti-inflammatory [14,15] antiviral [16] or antibacterial [17,18] activity. They act as hypolipoproteinemic and antiatherosclerotic agents [19] and are of benefit as pharmaceutical agents, especially in the treatment of adverse inflammatory, autoimmune, cardiovascular, proliferative and nociceptive conditions [20]. Hayakawa et al. have evaluated the functional groups connected to the central fused ring and their positions in terms of biological activity [21–23]. They found that the cytotoxicity of compound **A** decreased when the amino group was masked with one methyl group (**B**) (Fig. 1). On the other hand, the cytotoxicity had completely disappeared when the amino group was masked with two methyl groups. These results revealed that the functional groups contributed mainly to the biological activity and the central fused ring and its substituents are important. In this study, we have inserted another amine in addition to other substituents in the benzene ring and also inserted ethyl ester moiety instead of the phenyl ketone moiety (**DATP$_{a-c}$** Scheme 1) to investigate the relationship between the structure and biological activity of the derivatives. Also, the solubility and the accessibility are important factors for controlling the reactivity of any drug and thus thieno[2,3−*b*]pyridine derivatives **DATP$_{a-c}$** (Scheme 1) were loaded on chitosan nanoparticles to give the thienopyridines−CS nanocomposite (**CS−DATP$_{a-c}$**). The *in vitro* release studies of **CS−DATP$_{a-c}$**

* Corresponding author.
E-mail addresses: mansourhanaa@yahoo.com, hanaa.mansour@sci.kfs.edu.eg (H. Mansour).

https://doi.org/10.1016/j.carres.2020.107990
Received 11 February 2020; Received in revised form 10 March 2020; Accepted 23 March 2020
Available online 29 March 2020
0008-6215/

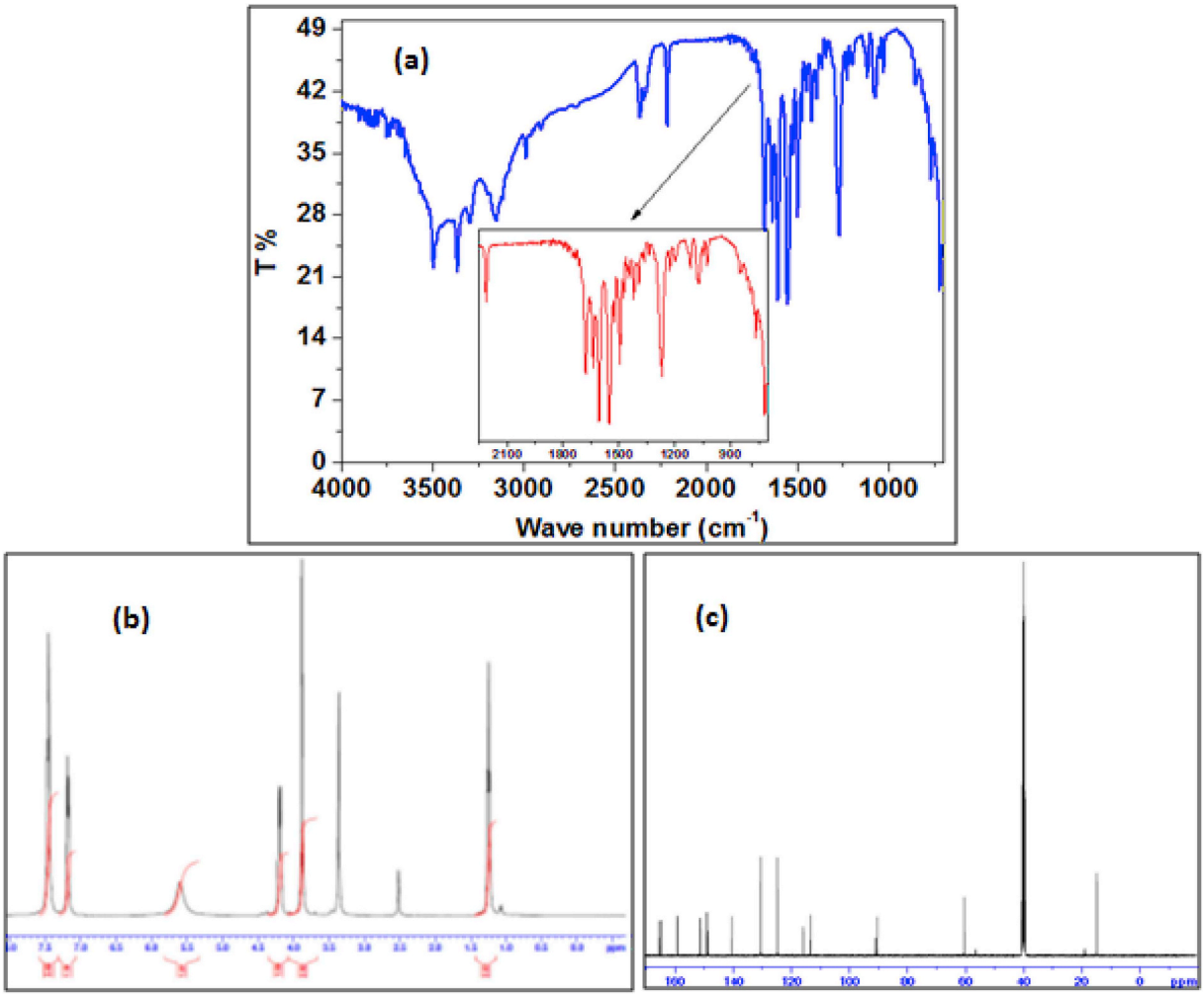

Fig. 1. a) FT − IR (KBr), b) ^{1}H NMR (DMSO − d_6) and c) ^{13}C NMR (DMSO − d_6) spectra of **DATP$_c$**.

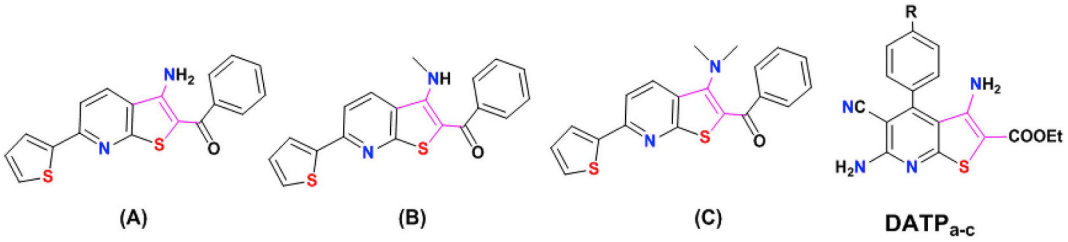

Scheme 1. Schematic representation of thieno[2,3 − *b*]pyridine derivatives **A**, **B**, **C** and **DATP$_{a-c}$**.

nanocomposites were investigated using the sonication method and UV–vis spectroscopy to investigate their pharmaceutical activities. The preliminary antibacterial activities of **DATP$_{a-c}$** and **CS − DATP$_{a-c}$** against *Escherichia coli*, *Salmonella choleraesuis*, *Staphylococcus aureus*, and *Proteus mirabilis* bacteria were tested *in vitro* and discussed.

2. Experimental part

2.1. Instrumentations

All reagents and solvents were used as purchased without further purification. Analytical TLC was performed using silica gel 60 F254 plates (Merck). Fourier transform infrared (FT − IR) spectra were obtained in the transmission mode using Mattson 1000, Unicam infrared spectrophotometer Cambridge, England. X − ray diffraction patterns (XRD) were obtained by Shimadzu 6000 instrument equipped with a Cu anode, automatic divergence slit and a graphite monochromator, under the following experimental conditions: CuKa radiation, 1.54 °A; generator tension, 45 kV; generator current, 40 mA; intensity ratio (a_2/a_1), 0.500. The morphology of the samples was examined using a transmission electron microscope (TEM) JEOL: JEM-100cx) to determine the particle size and particle shape. ^{1}H NMR spectra were obtained using Bruker DPX 400 MHz spectrometer with DMSO − d_6 as solvent and TMS as an internal reference. The UV − VIS spectra were obtained using PerkinElmer UV/VIS Lambda 2 spectrometer. Mass spectra were carried out using EI mode on Direct Inlet part to the mass analyzer in Thermo Scientific GCMS model ISQ at the Regional Center for Mycology and Biotechnology (RCMB), Al − Azhar University, Nasr City, Cairo.

2.2. Syntheses

2.2.1. Preparation of 6 − Amino − 3,5 − dicyano − 4 − (p − nitrophenyl) pyridin(1H) − 2 − thiones (III$_c$)

A mixture of arylidene malononitrile **I$_c$** (0.01 mol) and thiocyanoacetamide **II** (0.01 mol) in ethanol (50 ml) was refluxed in the presence of catalytic amounts of piperidine for 3 h. The solvent then was removed and the solid product, formed after the addition of diluted hydrochloric acid, was collected by filtration, washed with water and then recrystallized from ethanol. IR(KBr), cm^{-1}: 3350,3206 (NH_2); 2222 (CN); 1241(C═S); ^{1}H NMR (DMSO-d_6): δ (ppm) = 7.60 (br, 2H, NH_2); 13.02 (br,1H, NH); 7.60–8.30 (m, 4H, Ar–H); ^{13}C NMR (DMSO-d_6): δ (ppm) = 114.2,114.7 (CN); 123.0–157.3 (Ar–C); 197.8 (C═S).

2.2.2. General procedure for the preparation of compounds IV$_{a-c}$

Pyridinethiones (0.01 mol) was stirred at room temperature in DMF (7 ml) and KOH (10%, 2.7 ml) for 1 h. To this solution, ethyl chloroacetate (0.02 mol) was added dropwise with keeping the temperature at 25 °C. The reaction was monitored using TLC and at the end of the reaction, H_2O (5 ml) was added. The solid product formed was filtered off and washed with ethanol to give **IV$_{a-c}$**.

2.2.2.1. Ethyl 2 − (6 − amino − 3,5 − dicyano − 4 − phenylpyridin − 2 − thiolyl)acetate (IV$_a$).

IR(KBr), cm^{-1}: 3465, 3353 (NH_2); 2204 (CN); 1723(C═O$_{ester}$); ^{1}H NMR (DMSO-d_6): δ (ppm) = 1.22–1.25 (t, 3H, CH_3); 4.10 (s, 2H, CH_2); 4.15–4.20 (q, 2H, CH_2); 7.56–7.59 (m, 5H, Ar–H); 8.00 (s, 2H, NH_2 exchanged by D_2O); ^{13}C NMR (DMSO − d_6): δ (ppm) = 14.5 (CH_3); 32.4 (CH_2CO); 61.8 (CH_2); 115.5, 115.6 (CN); 128.4–166.0 (Ar–C); 168.5 (C═O).

2.2.2.2. Ethyl 2 − (6 − amino − 3,5 − dicyano − 4 − (p-methoxyphenyl) pyridin − 2 − thiolyl)acetate (IV$_b$).

IR(KBr), cm^{-1}: 3417, 3306 (NH_2) 2213(CN); 1731(C═O); ^{1}H NMR (DMSO-d_6): δ (ppm) = 1.21–1.25 (t, 3H, CH_3); 3.80 (s, 3H, OCH_3); 4.10 (s, 2H, CH_2); 4.13–4.19 (q, 2H, CH_2); 7.10–7.50 (m, 4H, Ar–H); 7.90 (s, 2H, NH_2 exchanged by D_2O); ^{13}C NMR (DMSO-d_6): δ (ppm) = 14.5 (CH_3); 32.4 (CH_2CO); 55.8 (OCH_3); 61.8 (CH_2); 115.5, 115.6 (CN); 126.2–165.9 (Ar–C); 168.5 (C═O).

2.2.2.3. Ethyl 2 − (6-amino − 3,5 − dicyano − 4 − (p − nitrophenyl)pyridin − 2 − thiolyl)acetate (IV$_c$).

IR(KBr), cm^{-1}: 3446, 3316 (NH_2), 2214(CN), 1742(C═O); ^{1}H NMR (DMSO-d_6): δ (ppm) = 1.22–1.25 (t, 3H, CH_3); 4.10 (s, 2H, CH_2); 4.17–4.33 (q, 2H, CH_2); 7.80–8.40 (m, 4H, Ar–H); 8.10 (s, 2H, NH_2 exchanged by D_2O); ^{13}C NMR (DMSO-d_6): δ (ppm) = 14.4 (CH_3); 32.4 (CH_2CO); 61.9 (CH_2); 115.2, 115.3 (2CN); 124.4–166.1 (Ar–C); 168.4 (C═O).

2.2.3. General procedure for the thienopyridines DATP$_{a-c}$

Compound **IV$_{a-c}$** (0.003 mol) was refluxed in sodium ethoxide (0.1 N) and the reaction was monitored by TLC. The solid product formed was collected by filtration and washed with ethanol.

2.2.3.1. 3,6 − diamino-4-phenylthieno − {2,3 − b}pyridines (DATP$_a$).

IR (KBr), cm^{-1}: 3501, 3353, 3297(NH_2); 2214 (CN); 1686 (C═O); ^{1}H NMR (DMSO-d_6): δ (ppm) = 1.23–1.26 (t, 3H, CH_3); 4.17–4.22 (q, 2H, CH_2); 5.50 (s, 2H, NH_2 exchanged by D_2O); 7.50–7.54 (m, 5H, Ar–H); 7.60 (s, 2H, NH_2 *exchanged by D_2O*); ^{13}C NMR (DMSO-d_6): δ (ppm) = 14,9 (CH_3); 60.3 (CH_2); 116.0 (CN); 128.4–159.2 (Ar–C); 165.3 (C═O).

2.2.3.2. 3,6 − diamino-4-(p-methoxyphenyl)thieno − {2,3 − b}pyridines (DATP$_b$).

IR(KBr), cm^{-1}: 3491, 3353, 3232 (NH_2); 2213 (CN); 1666 (C═O); ^{1}H NMR (DMSO − d_6): (ppm) = 1.22–1.26 (t, 3H, CH_3); 4.16–4.21 (q, 2H, CH_2); 5.60 (s, 2H, NH_2, *exchanged by D_2O*); 7.1 (s, 2H, NH_2); 7.20–7.40 (m, 4H, Ar–H); ^{13}C NMR (DMSO − d_6): δ (ppm) = 14,9 (CH_3); 56.5 (OCH_3); 60.2 (CH_2); 116.2 (CN); 125.6–160.8 (Ar–C); 165.3 (C═O).

2.2.3.3. 3,6 − diamino − 4 − (p − nitrophenyl)thieno − {2,3 − b}pyridines (DATP$_c$).

IR(KBr), cm^{-1}: 3501, 3430, 3366 (NH_2); 2215(CN); 1651(C═O); ^{1}H NMR (DMSO-d_6): δ (ppm) = 1.22–1.28 (t, 3H, CH_3); 4.17–4.22 (q, 2H, CH_2); 5.50 (s, 2H, NH_2 *exchanged by D_2O*); 7.50 (s, 2H, NH_2 exchanged by D_2O); 7.80–8.40 (m, 4H, Ar–H); ^{13}C NMR (DMSO − d_6): δ (ppm) = 14,60 (CH_3); 60.4 (CH_2); 115.8 (CN); 124.7–159.1 (Ar–C); 165.4 (C═O).

2.2.4. Synthesis of CS − DATP$_{a-c}$ nanocomposites

Thienopyridine derivatives **DATP$_{a-c}$** (0.0011 mol) was added to CS solution (1 g in 80 ml of 1% acetic acid) with stirring for 30 min. Then TPP (sodium tripolyphosphate) (1 g in 5 ml of water) was added during sonication for 15 min followed by stirring for 2 h. The products were separated using a centrifuge and dried at 40 °C.

2.3. In vitro drug release

The release study was carried out as follows: About 50 mg the sample was added to the buffer (50 ml) and the system was maintained at 37 °C throughout the study. A certain amount of the release medium was collected at appropriate intervals and the amount of drug was detected using a UV spectrometer at 378 nm. The percentage of drug release was calculated according to Equation (1).

$$\text{Drug released (\%)} = (A_t/A_\infty) \text{ x } 100 \quad (1)$$

Where A_t and A_∞ are the absorbances of releasing the drug at time *t* and the absorbance of a completely releasing drug, respectively.

2.4. Antibacterial activity

The groups of bacteria *Escherichia coli*, *Pseudomonas aeuroguinsa* (Gram-negative bacteria) and *staphylococcus aureus*, *Enterococcus faecalis* (Gram-positive bacteria) were used to investigate the antibacterial activities of the thienopyridines and their nanocomposites. Cut plug method, recorded by Pridham et al. 1956 [24], was used as follows: Freshly prepared spore suspension of different test microorganisms (0.5 ml of about 10^6 cells/ml) was mixed with 9.5 ml of nutrient agar medium (for bacteria) at 45 °C, poured on sterile Petri dishes, and left to solidify at room temperature. Regular wells were made in the inoculated agar plates by a sterile cork borer of 0.7 mm diameter. Each well was filled with 20 mg of each tested powder. Three replicas were made for each test, and all plates were incubated at 32 °C for 24 h for bacteria. Then the average diameters of inhibition zones were recorded in centimeters and compared for all plates. MIC (minimal inhibitory concentration) was measured as follows: Half-fold serial dilutions were made for selected compounds to prepare concentrations of 10–70 mg/ml in distilled water and zero concentration was considered as a negative control. A previously prepared pure spore suspension of each test microorganism (0.5 ml of about 10^6 cells/ml) was mixed with 9.5 ml of each concentration in sterile test tubes, incubated at 32 °C for 24 h for bacteria, then optical density of growth was measured by spectrophotometer (Optima SP-300, Japan) at 620 nm for each incubated mixture, results were represented graphically, and MIC was recorded for each tested material [25].

3. Results and discussion

3.1. Synthesis and characterization of thienopyridine derivatives DATP$_{a-c}$

According to the pathway shown in Scheme 2, a stepwise of synthesis thienopyridines **DATP$_{a-c}$** was carried out under mild reaction

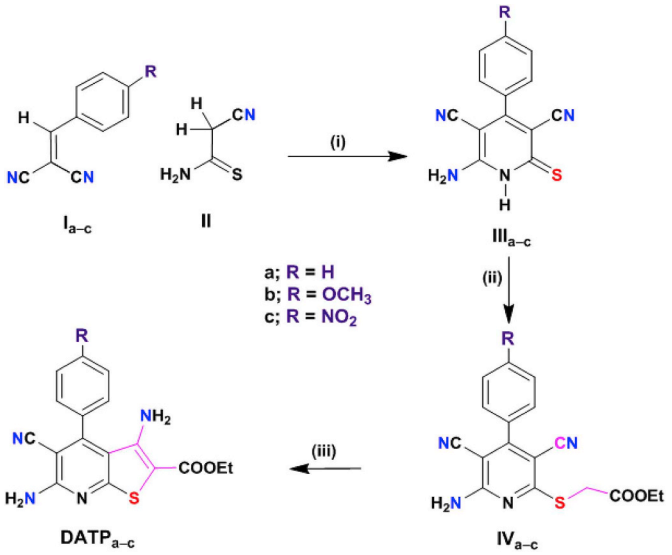

Scheme 2. Synthesis of the thienopyridine derivatives **DATP$_{a-c}$**; i) EtOH, piperidine, ii) $ClCH_2COOEt$, KOH, DMF; iii) Sodium ethoxide.

conditions based on Thorpe-Ziegler Cyclization [26]. Firstly, and according to Knoevenagel procedure [27], the reaction of arylidene malononitrile derivatives **(I_{a-c})** with thiocyanoacetamide (**II**) in ethanol in the presence of a base (piperidine), 6 − amino − 3,5 − dicyano − 4 − aryl − pyridine − 2(1*H*) − thione derivatives (**III_{a-c}**) were obtained in a high percentage yield. Different spectroscopic techniques were used to confirm the formation of **III_{a-c}** and the structures of compounds **III_a** and **III_b** are similar to that reported previously [28]. IR absorption spectrum of **III_c** shows characteristic bands at 3350, 3266, 2222 and 1241 cm^{-1} assigned for NH_2, NH, cyano and C═S groups, respectively. The ^1H NMR spectrum of **III_c** exhibits bands at δ = 7.60 and 13.02 ppm assigned for the NH_2 and NH protons (*exchanged by D_2O*). The aromatic protons appear at δ = 7.60–8.30 ppm. The ^{13}C NMR spectrum of **III_c** shows two bands at δ = 114.2 and 114.7 ppm assigned for the two cyano groups. The C═S group appears at δ = 197.8 ppm, whereas, the aromatic carbons appear at δ = 123.0–157.3. 2 − Alkylthio − 3,5 − dicyanoaminopyridines **(IV_{a-c})** were obtained by alkylation of 3,5 − dicyanoaminopyridine − 2(1*H*) − thiones **(III_{a-c})** using ethyl chloroacetate in basic medium.

The structure of the isolated 2 − alkylthio − 3,5 − dicyano-aminopyridines **(IV_{a-c})** was confirmed by different analytical methods. IR spectrum of **IV_b** shows the appearance of a new band at 1731 cm^{-1} assigned for CO_{ester}. The NH_2 group appears at 3417 and 3306 cm^{-1}, while the cyano groups appear as a sharp band at 2213 cm^{-1}. ^1H NMR (DMSO-d_6) spectrum of **IV_b** exhibits a triplet at δ = 1.21–1.25 ppm and a multiplet at δ = 4.13–4.19 ppm assigned for the CH_3 and CH_2 protons of the ethyl group, respectively. Two singlet bands appear at δ = 3.80 and 4.10 ppm assigned for the OCH_3 and S–CH_2 protons, respectively. The aromatic protons appear as a multiplet at δ = 7.10–7.50 ppm. The amine protons appear as a singlet band at δ = 7.90 ppm (exchanged by

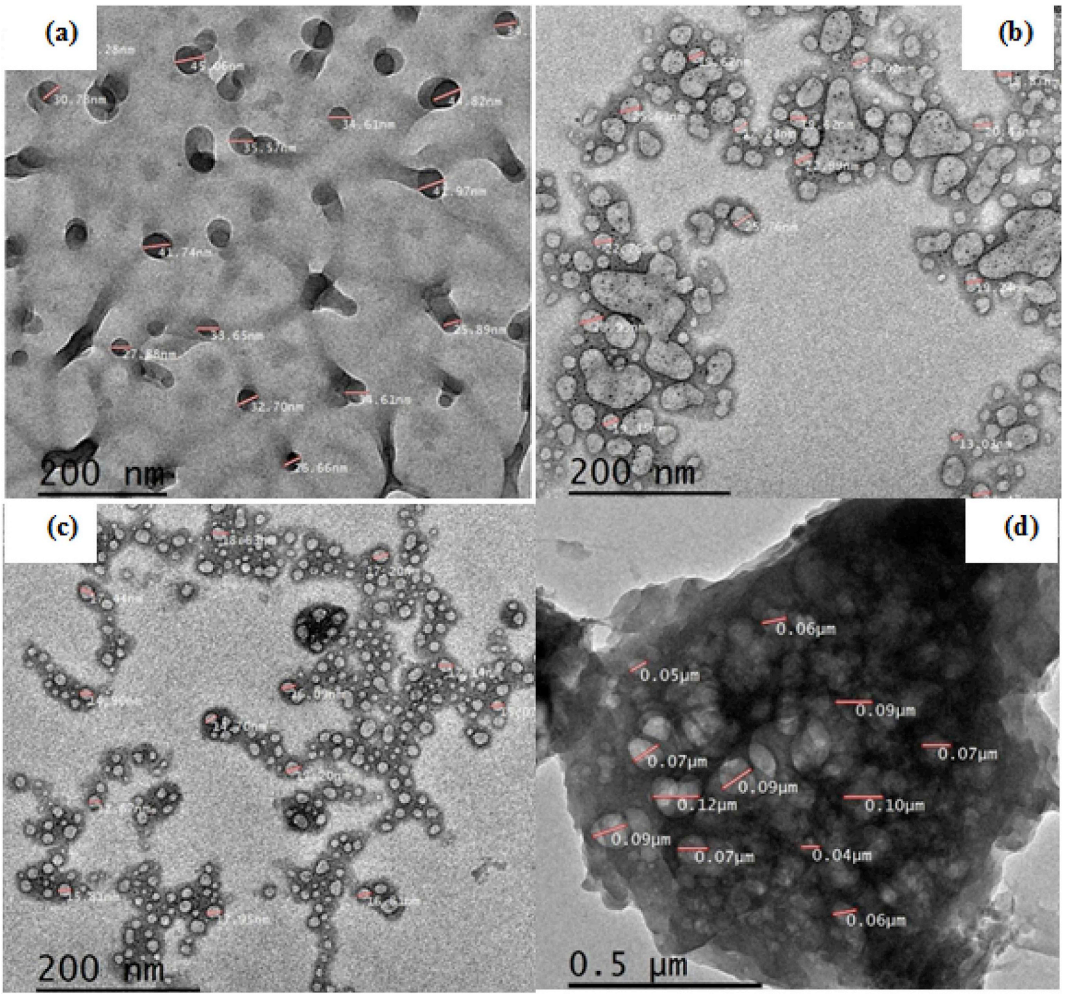

Fig. 2. TEM micrographs of **CS − DATP** nanocomposites; a) **CS − DATP$_a$**, b) **CS − DATP$_b$**; c) **CS − DATP$_c$**; and d) **CS** nanoparticle.

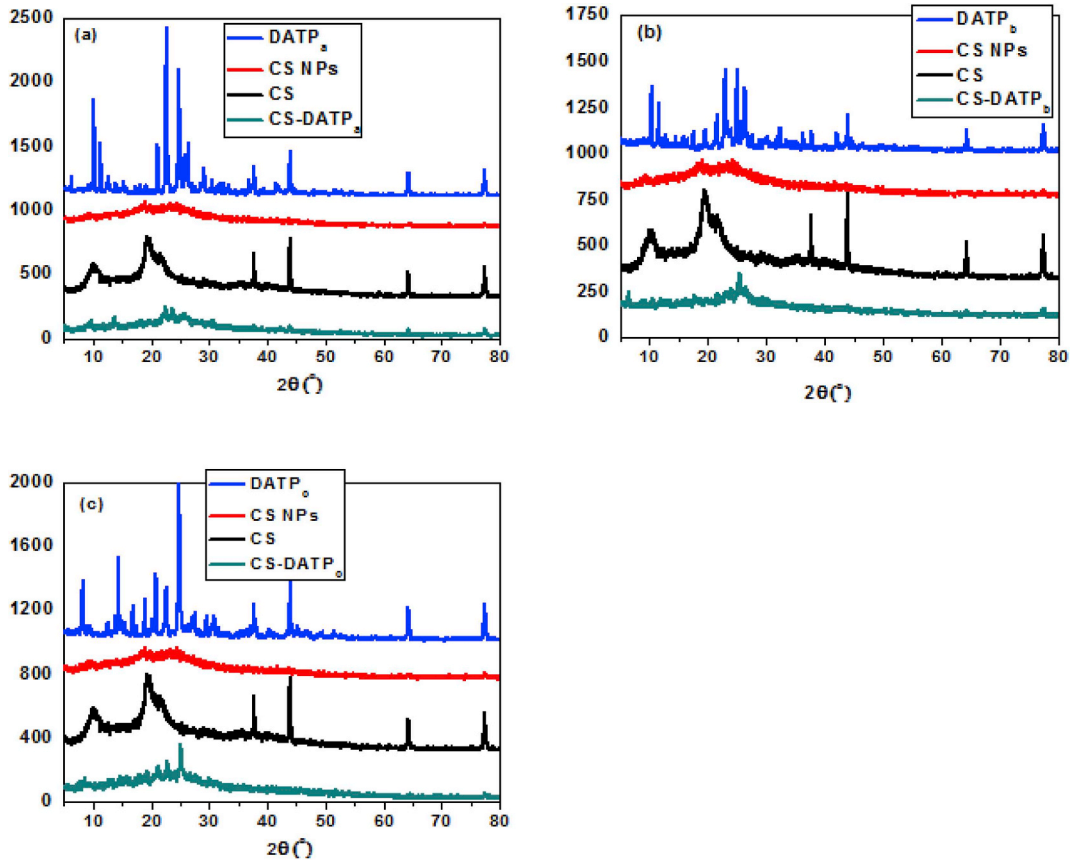

Fig. 3. XRD patterns of **DATP$_{a-c}$**, **CS − DATP$_{a-c}$** nanocomposites, chitosan and chitosan nanoparticles.

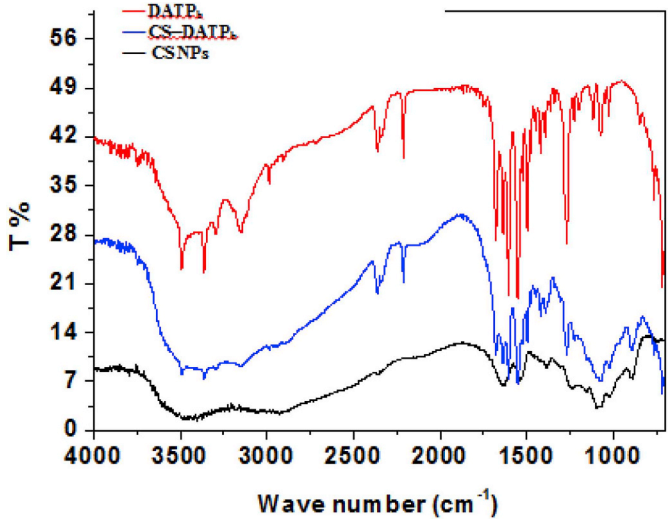

Fig. 4. FT-IR spectra of CS nanoparticles, **DATP$_b$** and **CS − DATP$_b$** nanocomposite.

D_2O), which is shifted to a higher field compared to the pyridine thione **III$_b$**. ^{13}C NMR spectrum confirmed the structure of **IV$_b$** which is distinguished by the disappearance of the C=S band at δ = 188.5 ppm and the appearance of a new band at δ = 168.5 ppm characteristic for the C = O_{ester}. The CH_3 and CH_2 carbons of the ester group appear at δ = 14.5 and 61.8 ppm respectively. A new band at δ = 32.4 ppm is characteristic for the (CH_2CO) group. The other bands have no distinguished changes as the (OCH_3) group appears at δ = 55.8 ppm, the two cyano groups found at δ = 115.5 and 115.6 ppm and the aromatic carbons are found at δ = 126.2–165.9 ppm. Thienopyridine **DATP$_{a-c}$** are generated by cyclization of 2-alkylthio-3,5-dicyano-aminopyridines (**IV$_{a-c}$**) in sodium ethoxide under reflux conditions. The structure of **DATP$_{a-c}$** is confirmed by IR, NMR, UV/Vis spectroscopy, mass spectrometry, and elemental analysis. IR spectrum of **DATP$_b$** (Fig. 1a) shows the C = O_{ester} at 1666 cm^{-1} which shows a large shift compared to the corresponding **IV$_b$**(1731 cm^{-1}), indicating for a new thieno ring formation. The amino groups appear at 3494, 3353 and 3232 cm^{-1} whereas; the cyano group appears as only one at 2213 cm^{-1}. The ^1H NMR spectrum of **DATP$_b$** (Fig. 1b) exhibits a triplet at δ = 1.22–1.26 ppm and a quartet at δ = 4.16–4.21 ppm, assigned for the CH_3 and CH_2 of the ester group. A new band appears as singlet band δ = 5.60 ppm for the newly formed amino protons (*exchanged by D_2O*), while the other amino appears at δ = 7.10 ppm (*exchanged by D_2O*). The aromatic protons appear as multiplet band at δ = 7.20–7.40 ppm. The ^{13}C NMR spectrum of **DATP$_b$** (Fig. 1c) is characteristic by the appearance of only one cyano carbon at δ = 116.2 ppm, while the other cyano group disappeared via the cyclization process. The ethyl ester carbons appear at δ = 14.9 and 60.3 ppm. The carbonyl carbon of the ester group is found at δ = 165.3 ppm. The methylene protons at δ = 32.4 ppm are disappeared via the new ring formation. The aromatic carbons are found at δ = 125.6–160.8 ppm. The UV/Vis spectrum of **DATP$_c$** is distinguished by the appearance of bands at λ_{max} = 327 nm. The EI − MS spectra of **DATP$_{a-c}$** showed the molecular ion peak, indicating the product formation.

3.2. Preparation and characterization of CS − $DATP_{a-c}$ nanocomposites

The morphology of **CS − DATP$_{a-c}$** nanocomposites was characterized by the TEM technique. The TEM image, depicted in Fig. 2, shows a relatively narrow size distribution of monodispersed nanopartiThe surface morphology characteristicscles with an average size of 14–78 nm. The spherical shape is due to the loading of the

Table 1
Zeta potential (mV) of **DATP$_{a-c}$** and **CS − DATP$_{a-c}$** nanocomposites.

Compound	DATP$_a$	DATP$_b$	DATP$_c$	CS − DATP$_a$	CS − DATP$_b$	CS − DATP$_c$
Zeta potential (mV)	−22.5	−27.5	−12.2	−0.8	+4.8	−9.4

thienopyridine derivatives with a deviation of ± 5 nm [29,30] have an impact on bioadhesion. It has been found that the nanospheres with a coarser and more porous surface may offer enhanced bioadhesivity as compared to those with a smoother texture.

It was reported that XRD spectra of pure chitosan have two prominent crystalline peaks at (2θ) of 10° and 20° assigned for the presence of plenty of OH and NH_2 groups that forms strong inter and intramolecular hydrogen bonds [31]. The XRD peak depends on the crystal size; but in the present study, for all the drug-loaded concentrations, the characteristic peak of thienopyridine could overlap with the polymer itself. Cross-linking Chitosan by TPP (Fig. 3) reveals the disappearance of peak at 10° and a shift of peak at 20° to 18° and a new broader one at 25° were observed. This could be attributed to the rearrangement of molecules in the crystal lattice. It was reported that after ionic cross-linking **CS** with TPP, no peak is detected in the diffractograms of **CS** nanoparticles, reflecting the destruction of the **CS** packing structure [32]. In the case of **CS − DATP$_{a-c}$** nanocomposites, several diffraction sharp peaks are observed at 10.4°, 12°, 16°, 21°, 22° and 25°due to the crystalline phase of the thienopyridine. Compared to **CS − DATP$_a$**, the sharp peaks for **DATP$_a$** were observed at the same positions indicating the inclusion of **DATP$_a$** in CS nanoparticles. Also, the peak for CS nanoparticles at 16° was shifted to 25°. Similar results were observed for the other thienopyridines (Fig. 3). This confirms the adsorption of the thienopyridines on the surface of CS nanoparticles. The peaks of the thienopyridines have disappeared after loading in the chitosan nanoparticles and this is in agreement with other results due to the encapsulation of thienopyridines in the polymer networks [32].

The FT − IR spectra of **DATP$_b$**, **CS − DATP$_b$** nanocomposites, and **CS** nanoparticles were recorded to observe the difference in structure due to DATP incorporation into the matrix (Fig. 4). The main characteristic peaks of the chitosan spectrum were: peaks at 3511 − 3491 cm^{-1} assigned to –O − H stretching; peaks at 3353 − 3374 cm^{-1} assigned to NH − and NH_2 − stretching and the peaks at 1639 cm^{-1} assigned for the amide stretching. Typical signals for saccharide structures appeared between 1205 and 900 cm^{-1} [33]. After the loading process, the IR spectra of **CS − DATP$_{a-c}$** showed some differences between the nanochitosan and those containing **DATP**. Especially, bands around 3490 cm^{-1}, typical for ν_{OH} and ν_{NH} became broader and shifted to about 3510 cm^{-1}. This indicated that the interaction is via the imino group of the chitosan moiety. Another feature showing the successful **DATP** loading was the shift of the amide band at 1639 to 1650 − 1666 cm^{-1}. The highly negative zeta potential of **DATP$_{a-c}$** compared to their **CS − DATP$_{a-c}$** nanocomposites insures the ability of capturing positively charged chitosan nanoparticles via ionic interactions (Table 1).

3.3. In vitro drug release

We investigate the potential applications of **CS − DATP$_{a-c}$** nanocomposite conjugates as pharmaceutically active compounds to

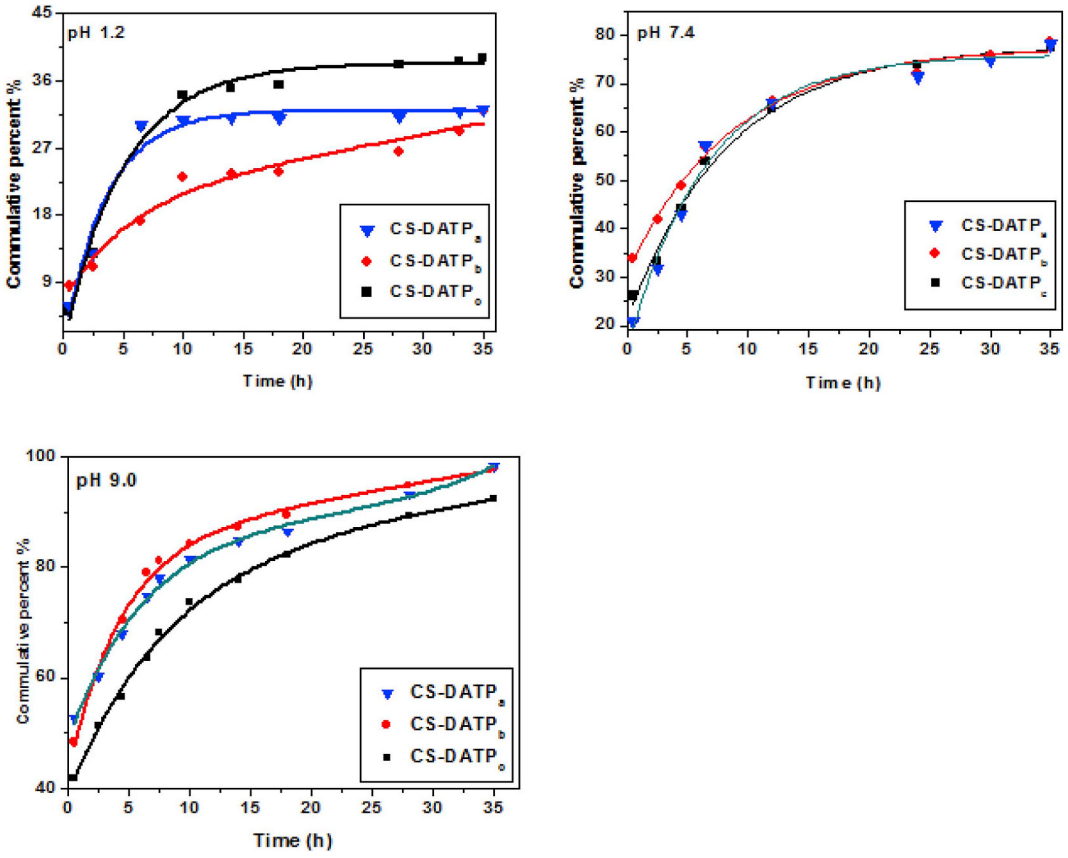

Fig. 5. Percentage cumulative release of different loading drugs as a function of time; at different pH media; a) pH = 1.2, b) pH = 7.4 and c) pH = 9.

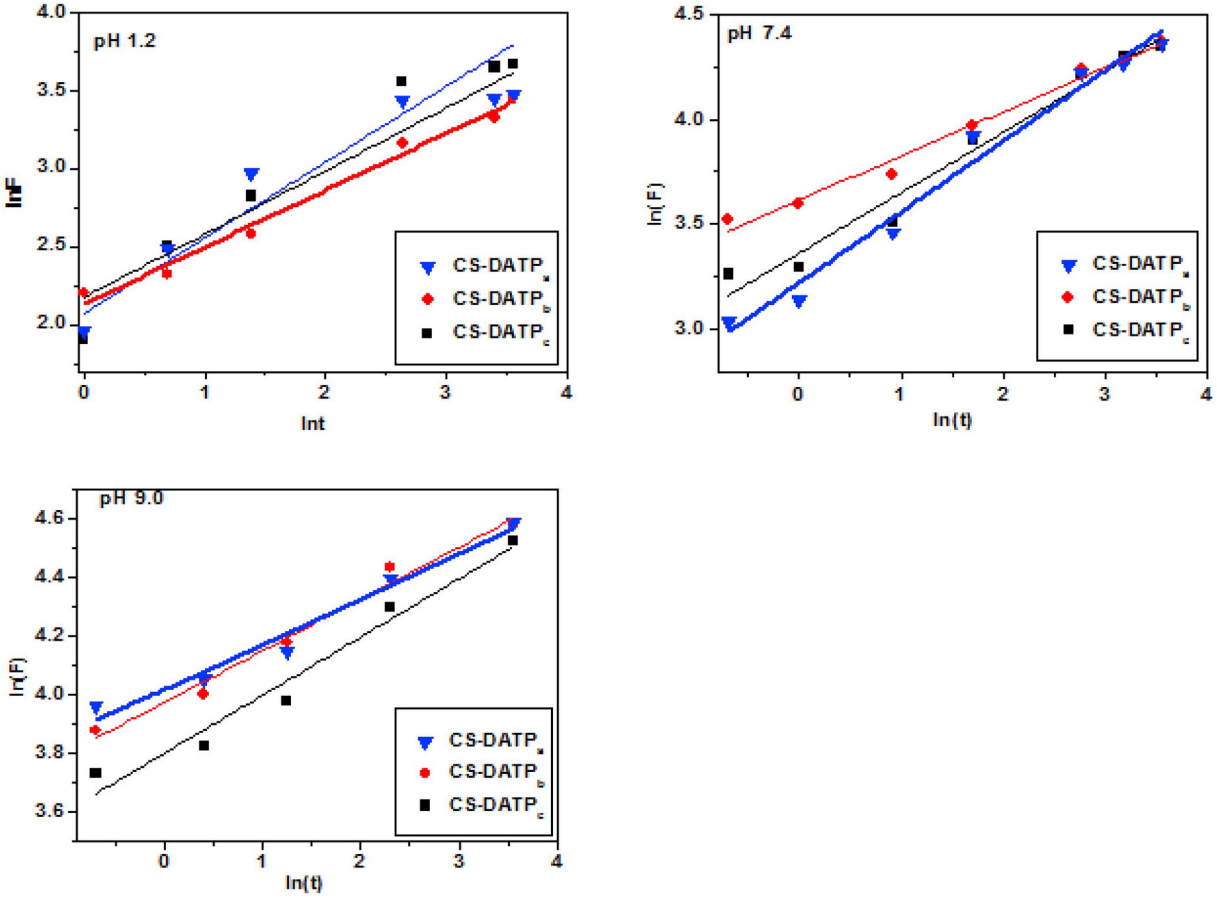

Fig. 6. Representation of the fractional released for all **CS − DATP$_{a-c}$** nanocomposites.

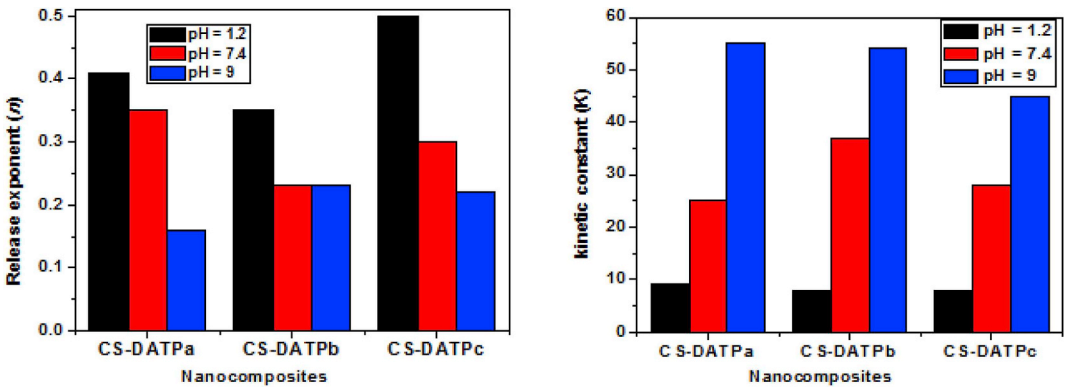

Fig. 7. Representation of release exponent (*n*) and kinetic constants (*K*) or drug release from the corresponding nanocomposites at 37 °C.

Table 2
Kinetic Constants (*K*) and release exponents (*n*) for drug release from the corresponding **CS − DATP$_{a-c}$** nanocomposites at 37 °C.

Compound	pH	*n*	*k*
CS − DATP$_a$	1.2	0.41	9
	7.4	0.34	25
	9	0.16	55
CS − DATP$_b$	1.2	0.37	8
	7.4	0.20	37
	9	0.18	54
CS − DATP$_c$	1.2	0.48	8
	7.4	0.29	28
	9	0.20	45

overcome the fast dissolution of chitosan in the stomach and also the limited capacity for controlling the release of drugs [34,35]. The *in vitro* hydrolysis behavior of **CS − DATP$_{a-c}$** nanocomposite was followed by monitoring the DATP using UV spectrophotometry at 378 nm during dissolution and diffusion in aqueous solution at different pH media [36,37]. The cumulative release rates of **CS − DATP$_{a-c}$** nanocomposites as a function of time (*t*) at different pH media are depicted in Fig. 5. Fig. 5 showed a first fast release step of **DATP** molecules and the release was trapped off with time. This is due to the increased difficulty of diffusion of the drug included inside the matrix with the decrease of the initial drug concentration in the crosslinked nanoparticles [38]. The release of **DATP** continues for 35 h, showing about 50%–70% of all **CS − DATP$_{a-c}$** nanocomposite. The release profile can be discussed as a rapid dissolution of **DATP$_{a-c}$** followed by release from the

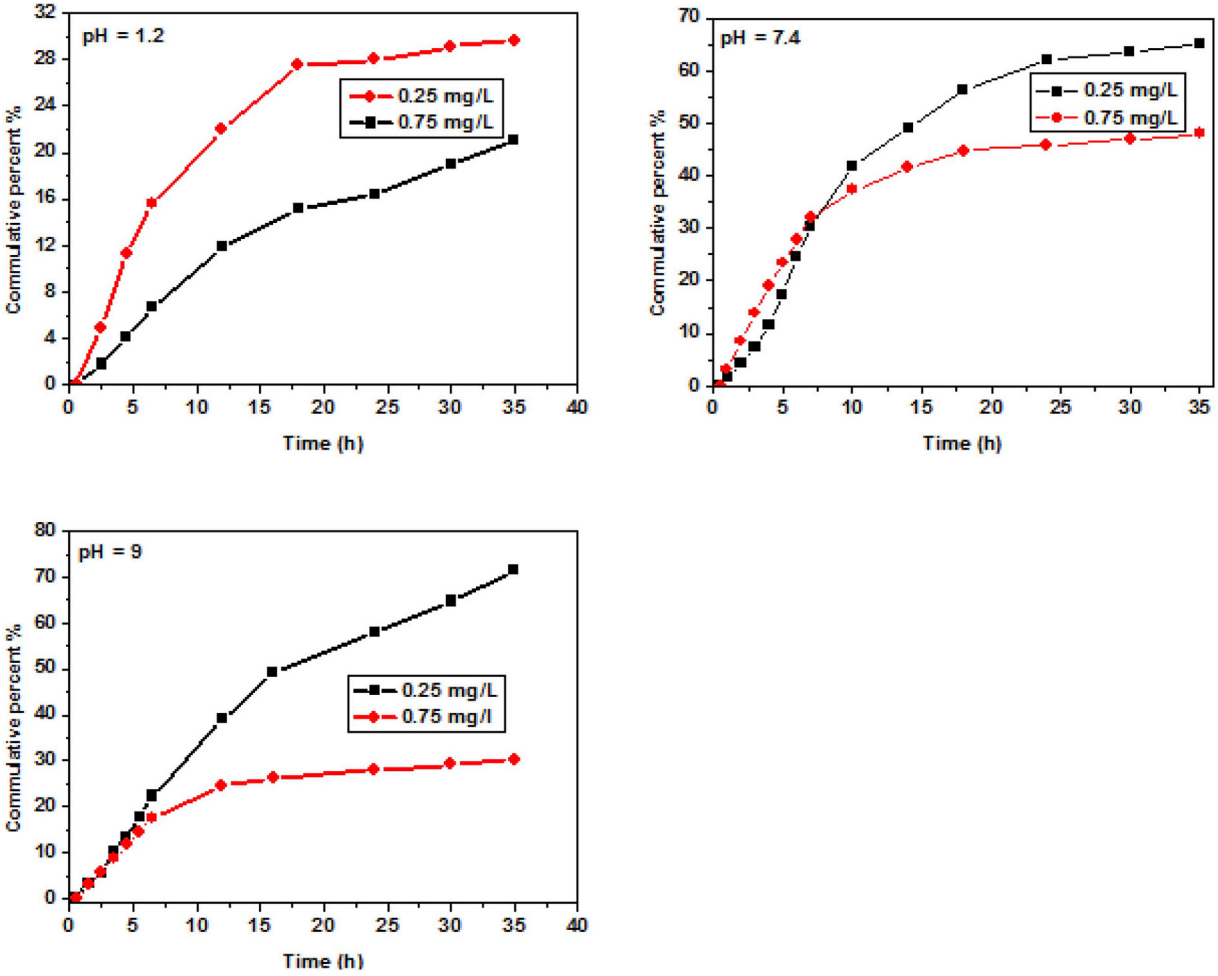

Fig. 8. Percentage cumulative release of **CS − DATP$_b$** nanocomposites in different concentrations a) 0.75 mg/L; b) 0.25 mg/L as a function of time and pH.

Table 3
Inhibition zone values of **DATP$_{a\text{-}c}$** and **CS − DATP$_{a-c}$** nanocomposites against gram-negative (*E. coli and P. aeruginosa)* and gram-positive (*S. aureus and E. faecalis)* bacteria (μg/ml).

	E. Coli	P. aeuroguinsa	S. aurins	E. Faecalis
DATP$_a$	0	0	6	0
DATP$_b$	5	0	5	4
DATP$_c$	6	1	5	5
CS − DATP$_a$	15	11	20	8
CS − DATP$_b$	16	8	8	10
CS − DATP$_c$	18	10	10	10

nanocomposites [39]. Effect of pH media on the drugs release behaviors were investigated and the drug release rate trend in different pH media is as follow: basic > neutral > acidic (Figs. 6 and 7). In acidic medium, most of the amino groups in the nanocomposites were protonated and the hydrogen bonds between matrix and **DATP** will be more favorable. The fast release rate in basic medium, compared to acidic and neutral, prolongs drug delivery in gastric pH. This would decrease physiological toxicity resulting from the fast release of the drug and may find biomedical applications. To investigate the release mechanism, the data were analyzed using Korsmeyer-Peppas Equation (2) [40,41].

$$F = M_t/M_\infty = kt^n \rightarrow lnF = lnK - n\ lnt \quad (2)$$

where the release fraction (F) is defined as M_t/M_∞, M_t is the amount of **DATP** drug released at any given time, M_∞ is the maximum amount

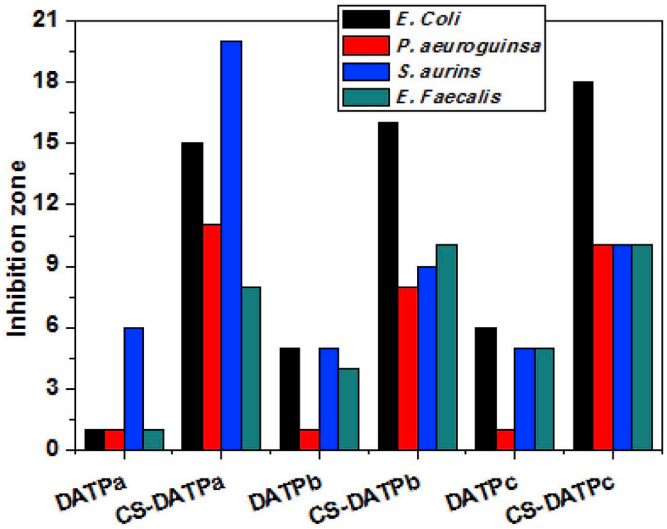

Fig. 9. Inhibition zone values against gram negative (*E. coli and P. aeruginosa)* and gram positive (*S. aureus and E. faecalis)* bacteria (μg/ml).

(weight) available for release, t is the release time, k is a constant related to the properties of the drug delivery system, and n is the release exponent. It was reported that one of the following four mechanisms are valid for drug release and this depends on the exponent n value [41]; i) diffusion through the matrix by a Fickian diffusion mechanism ($n < 0.5$); ii) non-Fickian mechanism ($0.5 < n < 1$); iii) a zero-order

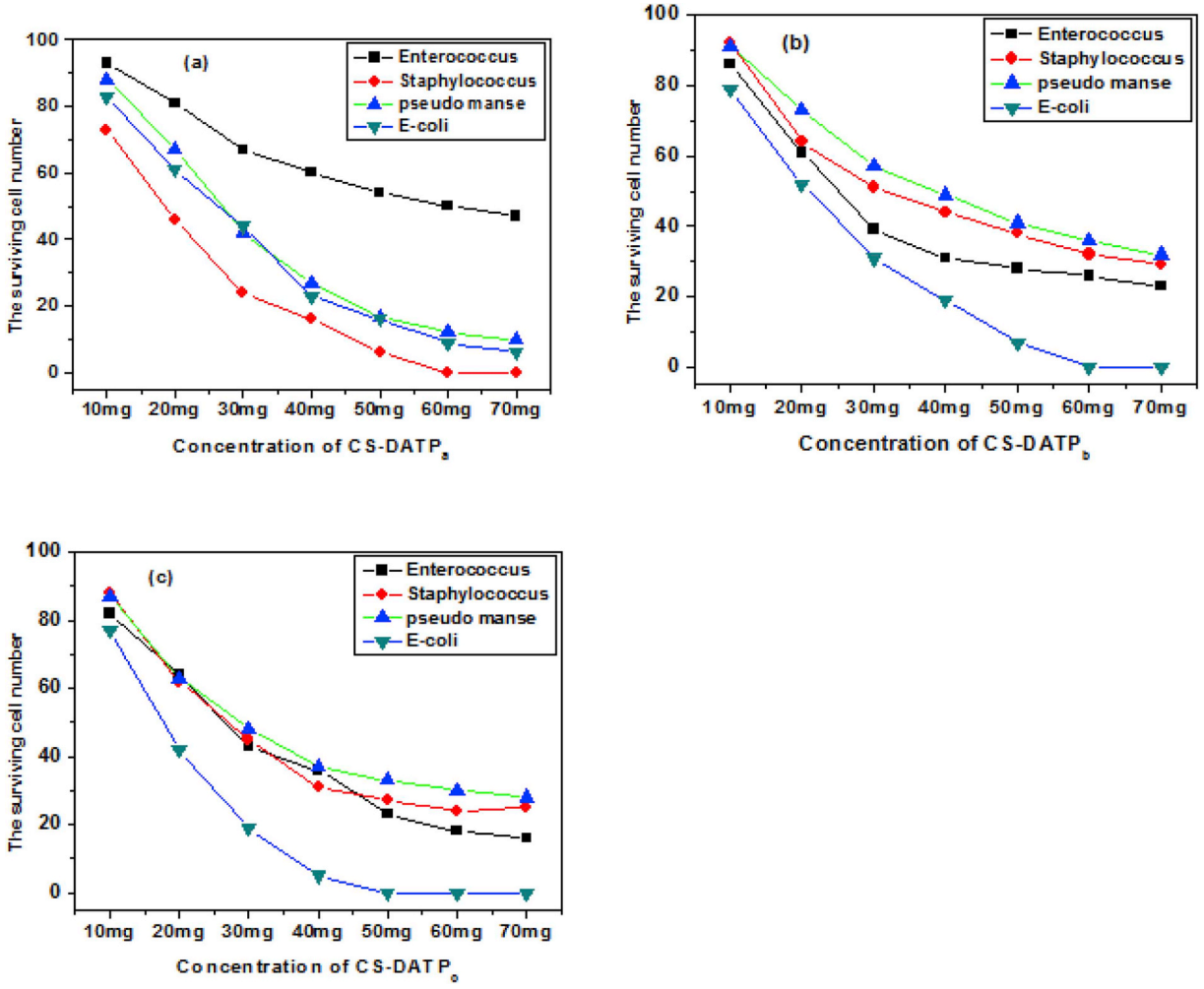

Fig. 10. The surviving cell number values versus concentrations of nanocomposites against gram-negative (*E. coli and P. aeruginosa)* and gram-positive (*S. aureus and E. faecalis)* bacteria (μg/ml).

mechanism ($n = 1$) and non-Fickian super release mechanism ($n > 1$). In our case, the n values, determined from Eq. (2), shown in Table 2, is < 0.5. This suggests a Fickian diffusion mechanism for all drugs release from the nanoparticles.

This behavior suggests that the release process is controlled by diffusion only [42] as the solvent mobility is very low in comparison to the relaxation rate. The release results will ensure the maximum availability of the drugs in the colon.

Fig. 8 showed that the drug release is dependent on the concentration of nanocomposites. Drug release behavior is prevented by inter-ionic interaction, which is related to nano chitosan concentration. As the nano chitosan concentration increases, the crosslinking density increases due to electrostatic attraction of a larger amount of nano chitosan with tripolysodium phosphate as a crosslinker agent, and as a result, physical entanglement among chitosan chains leads to the compact core and compact polyelectrolyte complex film. These factors would be expected to slow drug release–erosion process [43]. Therefore, the slower release rate for **CS − DATP$_b$** nanocomposites obtained at higher chitosan concentration can be easily understood.

3.4. Antibacterial activity

In the present study, the antibacterial property of the **CS − DATP$_{a-c}$** nanocomposites was evaluated against Gram − negative *(E. coli, P. aeuroguinsa) and* Gram-positive bacteria (S. *aureus*, *E. faecalis)* and compared with **DATP$_{a-c}$**. It was found that the diameter of the inhibition zone varied according to the active group in the copolymer and also the examined microorganism (Table 3). All bacteria were exposed to different concentrations of the tested compounds with duration of 24 h and the results are shown in Figs. 9 and 10. The results showed that: i) the effects of compounds depend on the concentration and the survival of bacteria increases with increased concentration of compounds (Fig. 10); ii) the diameter of inhibition zone and the MIC, the minimal inhibitory concentration, the lowest concentration of the antimicrobial that will inhibit the visible growth of microorganisms, varied slightly according to the active group of both **DATP$_{a-c}$** and **CS − DATP$_{a-c}$** nanocomposites and also the examined microorganism; iii) **CS − DATP$_{a-c}$** nanocomposites exhibited better activity against both Gram-positive and Gram − negative bacteria compared to **DATP$_{a-c}$**. The higher antibacterial activity of **CS-DATP$_{a-c}$** nanocomposites compared to **DATP$_{a-c}$** may be explained as follow: i) positively charged **CS − DATP$_{a-c}$** nanocomposites ($-NH_2^+$ on the C − 2 position of the D − glucosamine) can bind to bacterial cell surface which is negatively charged and disrupt the normal functions of the membrane, e.g. by promoting the leakage of intracellular components or by inhibiting the transport of nutrients into cells [44]; ii) or being adsorbed to the cell membrane through electrostatic interactions, probably by hydrophobic bonds or hydrogen bridges, being this adsorption concentration − dependent causing precipitation and coagulation of cytoplasmic proteins and bacterial death [45–48]; iii) also, the association of thienopyridine in the **CS − DATP$_{a-c}$** nanocomposites may affect the size of the nanocomposite and improves the cellular uptake of the

thienopyridine because the antibacterial activity strongly depends on the particle size [6,48]. The results also indicated that Gram-positive bacteria were less sensitive to the thienopyridine-chitosan nanocomposites than Gram − negative bacteria. An explanation may be the different characteristics of the cell surfaces of bacteria. Gram-negative bacteria have a higher negative charge on the cell surface compared to Gram − positive bacteria. As a result of the higher negative charge on the cell surface, the interaction between Gram − negative bacteria and **CS − DATP$_{a-c}$** nanocomposites was stronger than that of Gram − positive bacteria [49,50].

4. Conclusion

Three thieno[2,3 − *b*]pyridine derivatives **DATP$_{a-c}$** have been synthesized and loaded on chitosan nanoparticles to give the **CS − DATP$_{a-c}$** nanocomposites. **CS − DATP$_{a-c}$** nanocomposites show a relatively narrow size distribution of monodispersed nanoparticles with an average size of 14–78 nm. The *in vitro* release studies of **CS − DATP$_{a-c}$** nanocomposites were investigated and showed the drug release rate is independent of the benzene ring substituent but in turn, is pH-dependent and the trend is as follow: basic > neutral > acidic. The faster release rate in basic medium effectively prolongs drug delivery in gastric pH. Additionally, the antibacterial investigation showed that: i) Compound **DATP$_c$,** containing a withdrawing group, showed higher antibacterial compared to that containing a donor group or unsubstituted ring; ii) **CS − DATP$_{a-c}$** nanocomposites exhibited much higher antibacterial activity against both Gram − positive and Gram-negative bacteria compared to **DATP$_{a-c}$**. The association of thienopyridines in the **CS-DATP$_{a-c}$** nanocomposites affects the size of the nanocomposites and improves the cellular uptake of the thienopyridines as the antibacterial activity strongly depends on the particle size. The obtained results may have biological applications, especially as colon drug targeting.

Declaration of interests

The authors declare that they have no known competing financial interests or personal relationships that could have appeared to influence the work reported in this paper.

Declaration of competing interest

The authors declare that there are no conflicts of interest regarding the publication of this research paper.

References

[1] A.I. Qureshi, R.D. Cohen, Adv. Drug Deliv. Rev. 57 (2005) 281–302.
[2] M.N.V.R. Kumar, React. Funct. Polym. 46 (2000) 1–27.
[3] M.D. Dhanaraju, K. Bhaskar, C. Vamsadhara, Indian Drugs 40 (2003) 99–103.
[4] M.L. Lamosa, C. Lopez, J.L. Jato, M.J. Alonso, J. Contr. Release 52 (1998) 109–118.
[5] A. Anitha, S. Maya, N. Deepa, K. Chennazhi, S. Nair, H. Tamura, R. Jayakumar, Carbohydr. Polym. 83 (2) (2011) 452–461.
[6] N.Z. Shaban, S.A. Yehia, K.R. Shoueir, S.R. Saleh, D. Awad, S.Y. Shaban, J. Mol. Liq. 287 (2019) 111002–111010.
[7] W. Steinkopf, G. Lutzkendorf, Chem. Ztg. 36 (1913) 379–384.
[8] A. Krauze, S. Grinberga, L. Krasnova, I. Adlere, E. Sokolova, I. Domracheva, I. Shestakova, Z. Andzans, G. Duburs, Bioorg. Med. Chem. 22 (2014) 5860–5870.
[9] F. Ma, J. Liu, T. Zhou, M. Lei, J. Chen, X. Wang, Y. Zhang, X. Shen, L. Hu, Eur. J. Med. Chem. 152 (2018) 307–317.
[10] X.X. Zeng, R.L. Zheng, T. Zhou, H.Y. He, J.Y. Liu, Y.L. Zheng, Y. Yang, Bioorg. Med. Chem. Lett 20 (2010) 6282–6285.
[11] I. Hayakawa, R. Shioya, T. Agatsuma, H. Furukawa, Y. Sugano, Bioorg. Med. Chem. Lett 14 (2004) 3411–3414.
[12] I. Pevet, C. Brule, A. Tizot, Cruzalegui F. GohierA, J.A. Boutin, S. Goldstein, *Bioorg. Med. Chem.* Lett 19 (2009) 2517.
[13] J.P. Wu, R. Fleck, J. Brickwood, A. Calapilo, K. Catron, Z.D. Chen, T.A. Kelly, Bioorg. Med. Chem. Lett 19 (2009) 5547–5551.
[14] Sohda T, Makino H, Baba A. U.S. Patent 1998:5:747,486.
[15] T. Morwick, A. Berry, J. Brickwood, M. Cardozo, K. Catron, M. DeTuri, C.L. Cywin, J. Med. Chem. (2006) 2898–2905.
[16] M.E. Schnute, M.M. Cudahy, R.J. Brideau, F.L. Homa, T.A. Hopkins, M.L. Knechtel, J.L. Wieber, J. Med. Chem. 48 (2005) 5794–5804.
[17] M.M. El-Abadelah, S.S. Sabri, H.A. Al-Ashgar, Heterocycles 45 (1997) 255–260.
[18] B. Leal, I.F. Afonso, C.R. Rodrigues, P.A. Abreu, R. Garrett, L.C.S. Pinheiro, H.C. Castro, Bioorg. Med. Chem. 16 (2008) 8196–8204.
[19] Fujikawa Y, Suzuki M, Iwasaki H, Sakashita M, Kitahara M. US Patent 1991: 5:026, 698.
[20] Brooking DC, Huchings MC, Langham BJ *WO Patent* 2009: 093008 A1.
[21] I. Hayakawa, R. Shioya, T. Agatsuma, H. Furukawa, Y. Sugano, Bioorg. Med. Chem. Lett 14 (2004) 3411–3414.
[22] S.I. Moryashova, L.K. Salamandra, A.E. Fedorov, L.A. Rodinovskaya, A.M. Shestopalov, V.V. Semenov, Russ. Chem. Bull. 47 (1998) 357–360.
[23] S.I. Moryashova, L.K. Salamandra, A.E. Fedorov, L.A. Rodinovskaya, A.M. Shestopalov, V.V. Semenov, Izv. Akad. Nauk, Ser. Khim. 2 (1998) 365–370.
[24] T. Pridham, L. Lindenfelser, O. Shotwell, F. Stodola, R. Benedict, C.J. Foley, Phytopathology 46 (1956) 568–575.
[25] Shadomy S, Epsinel I, Cartwright R: Laboratory studies agents: Susceptibility test and bioassays. In: Lennette A, Balows W, Hausler H, Shadomy S. fourth ed. Of: Manual of Clinical Microbiology, 1985: Little Brown Co., Boston.
[26] A. Krauze, I. Grinberga, L. Krasnova, I. Adlere, E. Sokolova, Shestakova II, Z. Andzans, G. Duburs, Bioorg. Med. Chem. 22 (2014) 5860–5870.
[27] G. Jones, Org. React. 15 (1967) 204–599.
[28] A.A. Geies, A.M. Kamal El-Dean, M.I. Abdel Monem, Z. Naturforsch. 47b (1992) 1438–1440.
[29] R.P.E. Muhammed, V. Junise, R. Saraswathi, P.N. krishnan, C. Dilip, Res. J. Pharmaceut. Biol. Chem. Sci. 1 (4) (2010) 383–390.
[30] M.H. Kafshgari, M. Khorram, M. Khodadoost, S. Khavari, Iran. Polym. J. (Engl. Ed.) 20 (5) (2011) 445–456.
[31] S.W. Ali, S. Rajendran, M. Joshi, Carbohydr. Polym. 83 (2011) 438–446.
[32] R. Yoksan, J. Jirawutthiwongchai, K. Arpo, Colloids Surf., B 76 (2010) 292–297.
[33] S. Tamburaci, F. Tihminlioglu, Mater. Sci. Eng. 80 (Supplement C) (2017) 222–231.
[34] P.M. de la Torre, EnobakhareY, G. Torrado, S. Torrado, Biomaterials 24 (2003) 1499–1506.
[35] Machluf M1, J. Kost, J. Biomater. Sci. Polym. Ed. 5 (1–2) (1993) 147–156.
[36] M. Ishihara, K. Obara, T. Ishizuka, M. Fujita, M. Sato, K. Masuoka, Y. Saito, H. Yura, T. Matsui, H. Hattori, M. Kikuchi, A. Kurita, J. Biomed. Mater. Res. 64A (2003) 248–256.
[37] Y. Tabata, Y. Ikada, Biomaterials 20 (1999) 2169–2175.
[38] A.A.A. de Queiroz, G.A. Abraham, O.Z. Higa, Acta Biomater. 2 (2006) 641–650.
[39] M. Babazadeh, L. Edjlali, L. Rashidian, J. Polym. Res. 14 (2007) 207–213.
[40] P. Costa, Int. J. Pharm. 220 (2001) 77–83.
[41] P. Costa, J.M.S. Lobo, Eur. J. Pharmaceut. Sci. 13 (2001) 123–133.
[42] J. Berger, M. Reist, J.M. Mayer, O. Felt, N.A. Peppas, R. Gurny, Eur. J. Pharm. Biopharm. 57 (2004) 53–63.
[43] S. Chen, M. Liu, S. Jin, B. Wang, Int. J. Pharm. 349 (2008) 180–187.
[44] I.M. Helander, E.-L. Nurmiaho-Lassila, R. Ahvenainen, J. Rhoades, S. Roller, Int. J. Food Microbiol. 71 (2001) 235–244.
[45] L.G. Hjeljord, G. Rolla, P. Bonesvoll, J. Periodontal. Res. Suppl. 12 (1973) 11–16.
[46] W.B. Hugo, A.R. Longworth, J. Pharm. Pharmacol. 16 (1964) 751–758.
[47] B. Melsen, O. Kaae, G. Rölla, O. Fejerskov, T. Karring, Arch. Oral Biol. 24 (1) (1979) 75–78.
[48] L. Zhang, Y. Jiang, Y. Ding, M. Povey, D. York, J. Nanoparticle Res. 9 (2007) 479–489 3.
[49] Y.C. Chung, Y.P. Su, C.C. Chen, G. Jia, H.L. Wang, J.G. Wu, J.G. Lin, Acta Pharmacol. Sin. 25 (7) (2004) 932–936.
[50] Z.X. Xue, G.P. Yang, Z.P. Zhang, B.L. He, React. Funct. Polym. 66 (9) (2006) 893–901.